ELSEVIER

Journal of Photochemistry and Photobiology A: Chemistry 145 (2001) 159–164

Journal of Photochemistry and Photobiology A:Chemistry

www.elsevier.com/locate/jphotochem

Nanosecond photo-fusion of microcrystals on a polymer film observed with time-resolved ultramicroscopy

Ken-ichi Saitow [a,1], Hiromi Banjo [a,b,2], Nobuyuki Ichinose [a,3], Shunichi Kawanishi [a], Hiroshi Masuhara [b], Hiroshi Fukumura [a,b,*]

[a] *Advanced Science Research Center, Japan Atomic Energy Research Institute, Neyagawa, Osaka 527-0019, Japan*
[b] *Department of Applied Physics, Osaka University, Suita 565-0871, Japan*

Abstract

A time-resolved ultramicroscope was developed to monitor the process of pulse-laser-induced melting of 9,10-dicyanoanthracene microcrystals on poly(ethyl methacrylate) films. The microscope can detect sub-micrometer particles, but with an image (spacial) resolution of 2 μm and a time resolution of 400 ps. Quantitative comparison between images obtained at a certain time delay after an excitation laser pulse and a pre-irradiated image is achieved using a correlation function. It was found that crystals having a size of about 10 μm turn in hot liquid droplets within the nanosecond excitation pulse after which 80% of the droplets solidify with a time constant of 9 ns. The residual 20% of hot liquid droplets appear to have either evaporated or fused and dispersed into the polymer with a time constant of 15 ns.

Keywords: Nanosecond photo-fusion; Time-resolved ultramicroscope; Laser-induced melting

1. Introduction

Intense pulsed laser irradiation of light absorbing molecular crystals or solid polymers generates a high density of electronically excited molecules. At sufficiently high laser fluence, the irradiated area's morphology becomes modified through photochemical or photophysical processes known as ablation [1]. Photochemically induced ablation can arise from photo-fragmentation of absorbing molecules caused by single photon or multiple photon events or sequences. Photophysical ablation is induced in systems where rapid non-radiative decay converts photon energy efficiently to thermal energy resulting in the release of considerable energy, which then flows into the molecular solid. This results in super heating of the irradiated area with transient temperatures of up to 1000 K being reported [2–4]. Such a temperature cannot be maintained by a molecular solid and rapid explosive phase change occurs. A polymer that is transparent to the excitation light can also be photo-ablated when doped with absorbing molecules [5–10]. In this case, the local temperature within the polymer around the dopant molecules has also been experimentally estimated to be 1000 K [8–10].

When the laser fluence is below the ablation threshold, other specific phenomena occur. For example, when a doped polymer film is irradiated at sub-ablation threshold, the dopant molecules can themselves be ejected from the heated polymer matrix [11]. A graphic illustration of this is obtained if a second, neat, polymer film is overlaid and tightly contacted with the doped film and the contacted films are then irradiated with a nanosecond pulsed laser. In this way, the dopant molecules alone can be space-selectively transferred from the source film into the target film. No transfer of other ablated material occurs if the conditions are carefully optimized [12–17]. This phenomenon has come to be known as laser molecular implantation and is schematically represented in Fig. 1. For implantation to occur, discrete mechanistic aspects exist. Molecular ejection must occur from the doped film followed by transfer from the doped film to the undoped film where crystallization or diffusion can occur. Subsequent laser pulses lead melting and diffusion into the undoped film.

* Corresponding author. Present address: Graduate School of Science, Tohoku University, Aoba, Aramaki, Aoba-ku, Sendai 980-8578, Japan. Tel.: +81-22-217-6567; fax: +81-22-217-6570.
E-mail address: fukumura@orgphys.chem.tohoku.ac.jp (H. Fukumura).
[1] Present address: Department of Diversity Science, Graduate School of Science and Technology, Chiba University, Yayoi, Inage, Chiba 263-8522, Japan.
[2] Present address: Toshiba Corporation, Manufacturing Engineering Research Center, Yokohama 235-0017, Japan.
[3] Present address: Department of Molecular Excitation Chemistry, The Institute of Scientific and Industrial Research, Osaka University, 8-1 Mihogaoka, Ibaraki, Osaka 567-0047, Japan.

1010-6030/01/$ – see front matter
PII: S1010-6030(01)00578-0

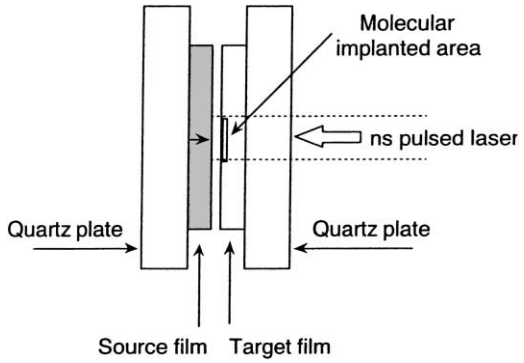

Fig. 1. Schematic diagram of laser molecular implantation.

Previous studies on the laser molecular implantation have clarified several features of the implantation process using static measurement techniques [12–17]. For example, the dopant molecule penetration depth into the neat film is tens of nanometers, the dopant molecule dispersion and mixing is on the molecular level, the polymer's glass transition is important as are the total energy input and energy input rates. Intermolecular interactions play an important role. Despite this widespread investigation, dynamic studies have not yet been reported. In order to investigate dynamic aspects of dopant molecule behavior pertinent to implantation dynamics as well as to understanding the fundamental principles of rapid pulsed laser-induced phase change, a sub-nanosecond time-resolved ultramicroscope was constructed for the present study. Using this instrument, 9,10-dicyanoanthracene (DCNA) microcrystals having a size of about 10 μm formed on a poly(ethyl methacrylate) (PEMA) film, were observed and time-resolved two-dimensional images were obtained of photo-induced phase transition from microcrystals to hot liquids induced by a single laser pulse followed by subsequent recrystallization. The time constants of these phase transitions were derived from a correlation function determined as a function of time. Some amount of the crystals (20%) was lost permanently to other processes such as evaporation and dispersion into the polymer.

2. Experimental

2.1. Sample preparation

Neat 6 wt.% PEMA in chloroform (Mw = 3.4×10^5) was spin coated onto quartz plates. At this concentration, the thickness of the films was 3 μm when using a spin rate of 1000 rpm. Doped ("source") films were prepared from a saturated solution of DCNA in PEMA–chloroform (6 wt.%). The doped film was overlaid onto the neat ("target") film and irradiated with a single shot of an XeF excimer laser (351 nm, FWHM = 30 ns) passing through the neat film as shown schematically in Fig. 1. The ablation threshold of the doped film was 400 mJ/cm^2 [17], so a fluence 150 mJ/cm^2 was chosen for excitation. DCNA from the doped film was transferred onto the neat film forming microcrystals of about 10 μm in size. This film with its microcrystals was then ready for the ultramicroscopic measurement to study the primary processes of pulsed laser driven melting, vaporization, recrystallization and dispersion (implantation) into the polymer matrix.

2.2. Time-resolved ultramicroscopy

A schematic diagram of the sub-nanosecond time-resolved ultramicroscope is shown in Fig. 2. The third harmonic (THG) of a nanosecond (4 ns, 15 mJ/pulse) Q-switched Nd^{3+}:YAG laser was used to excite DCNA microcrystals. The fundamental (1064 nm) of a picosecond Nd^{3+}:YAG laser (Lightwave 131) was amplified with a regenerative amplifier (Continuum RGA69-10) and doubled generating second harmonic (SHG) with a duration of 25 ps and a fluence of 25 mJ/pulse. The SHG was used to excite a rhodamine 101 (R101) solution producing the microscope's probe light. There are two reasons for this choice of probe light over the SHG itself. Firstly, using a coherent light source results in interference fringes and speckled images are formed in the ultramicroscope. Secondly, DCNA fluorescence occurs in the region of 532 nm and is, therefore, difficult to extract from the light caused by the pump beam alone. Fluorescence from R101 is sufficiently red shifted with respect to that from DCNA that with a suitable band-pass filter scattered probe beam alone is recorded in the image field.

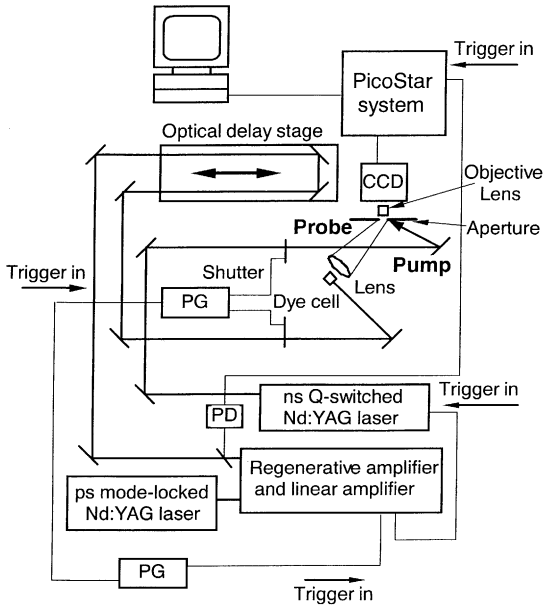

Fig. 2. The sub-nanosecond time-resolved ultramicroscope (PG is the digital pulse/delay generator and PD is the photodiode for the pulse induced trigger).

The probe light was focused at a tilted angle onto the polymer film. The tilt incidence angle allows the detection of scattered probe light alone (no direct light is detected). The scattered probe light was passed through a pinhole with a diameter of 5 mm and was then imaged through a lens onto a CCD camera equipped with a gated image intensifier with a gate width of 120 ps (PicoStar, Lavision GMBH). The CCD had 384 columns and 272 rows of pixels with each pixel representing 2 μm of the imaged field. The amplified picosecond Nd^{3+}:YAG laser was externally triggered at 1 Hz using a digital pulse/delay generator (Stanford Research System: DG535). The Q-switch on the nanosecond Nd^{3+}:YAG laser was synchronized by an electronic output from the regenerative amplifier, and the CCD camera gate was triggered optically by the arrival of a pulse from the picosecond Nd^{3+}:YAG laser. Shutters were triggered to chop the repetition rate at the sample to 0.2 Hz so that the sample could be easily translated between shots and data could then be accumulated from different regions. The instrumental response function was about 400 ps, because the fastest gate width of the CCD camera is 120 ps and the jitter between firing the nanosecond YAG and picosecond YAG is a few hundred picoseconds.

The picosecond Nd^{3+}:YAG's pulse arrival time was variable in the sub-nanosecond time scale using an optical delay line as well as in the longer timescale using the delay generator. Time-resolved data was collected from −10 to +30 ns. In order to analyze the time-resolved data, a full data set of images included those measured before, during and after excitation by a single nanosecond pump pulse.

3. Results and discussions

3.1. Time-resolved ultramicroscope images

An ultramicroscope enables us to probe inhomogeneity in a homogeneous medium, for example, micro-particles in solution and the Tyndall effect [18]. In the present experiment, the probed inhomogeneity corresponds to the microcrystals existing on the flat polymer surface. As a result, we can detect time-resolved laser-induced changes in the shape of the microcrystals through changes in the scattered light image in contrast to the dark background produced by the polymer film. Fig. 3(a) shows an example of the type of two-dimensional image that could be obtained from

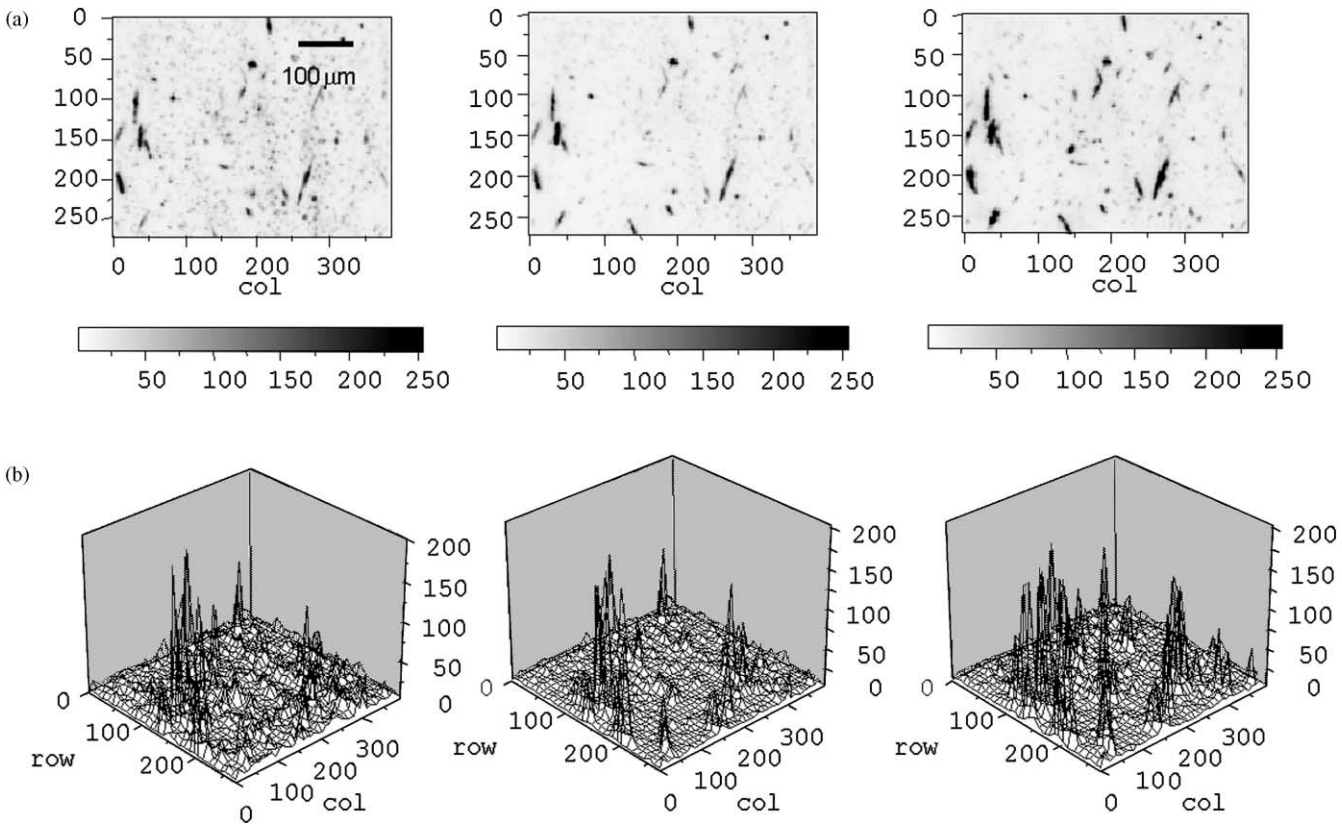

Fig. 3. Two-dimensional images of DCNA microcrystals formed on the target PEMA films measured by the ultramicroscope. The data is measured pre-irradiation, at $t = -1.5$ ns and at $t = +\infty$ after irradiation: (a) black points and white regions represent microcrystals and flat polymer surface, respectively; (b) counter map of scattering intensity as a function of pixel position on the CCD camera (columns = 384, rows = 272). The map is derived from (a).

the surface of a single sample film before, during, and after excitation with a single nanosecond laser pulse below the ablation threshold. Black points indicate bright scattering from microcrystals of DCNA with an averaged size of about 10 μm, and white areas represent dark regions from the homogeneous flat surface of target film. Contour maps of scattered light intensity shown in Fig. 3(a) are shown in Fig. 3(b). Both sets of figures indicate that microcrystals transiently disappear during the pulsed excitation although they have partially reappeared at infinite time. Importantly, a portion of the microcrystals has been permanently lost even at $t = +\infty$. Time-resolved images from −6 to +22 ns are displayed in Fig. 4, from which it is clear that the microcrystals disappear within the laser pulse, but then gradually reappear as the delay time after excitation becomes longer.

3.2. Image analysis using a correlation function

In order to investigate phase change dynamics of microcrystals, a correlation function is derived from the images obtained with the time-resolved microscope. The correlation function is calculated using the following equation.

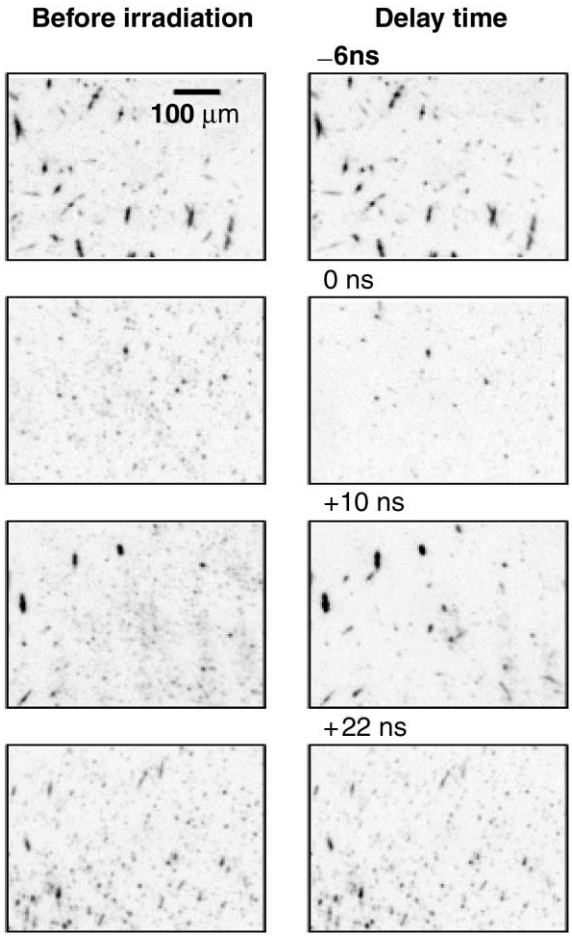

Fig. 4. Time-resolved images from the ultramicroscope after a single laser pulse. Delay times given are the time after excitation by a single nanosecond laser pulse.

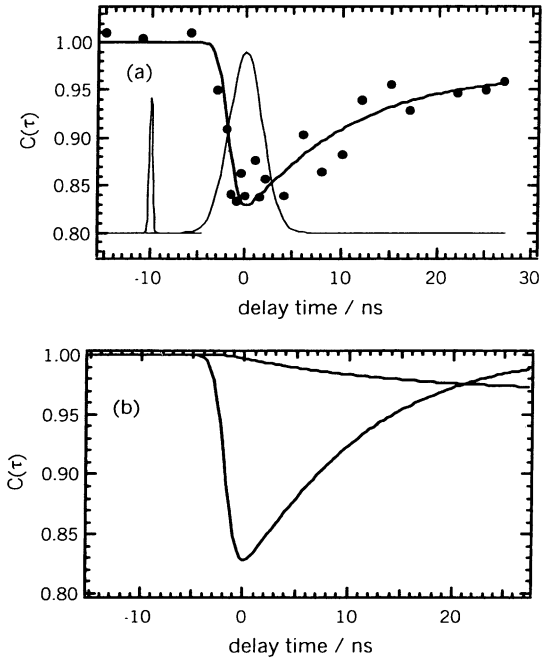

Fig. 5. Correlation functions for DCNA microcrystals excited by nanosecond pump pulses. (a) Correlation function fitted by a triple-exponential function convoluted with an instrumental response function. Solid, dashed, and thin lines are the fitting function, excitation pulse width and instrumental functions, respectively. (b) The decomposed correlation function.

$$C(t) = \frac{\sum_{i,j=0} I_{i,j}(0) I_{i,j}(t)}{\sum_{i,j=0} I_{i,j}(0)^2} \tag{1}$$

where $C(t)$ is the correlation function at time t, $I_{i,j}(0)$ and $I_{i,j}(t)$ are scattered intensities at $t = 0$ and t for each pixel on the CCD camera. Data for the variation of the derived correlation with time were fitted to the following equation.

$$C(\tau) = \int_{-\infty}^{\infty} f(\tau - t)\left(a + b\exp\left(\frac{-t}{\tau_1}\right) + c\exp\left(\frac{-t}{\tau_2}\right) + d\exp\left(\frac{-t}{\tau_3}\right)\right) \mathrm{d}t \tag{2}$$

The correlation function plotted as a function of time is shown as the solid line in Fig. 5(a) and the excitation pulse and the instrumental response functions are dashed and thin lines, respectively. Eq. (2) is a function consisting of a triple-exponential convoluted with the instrumental response function ($f(\tau - t)$) with an FWHM = 400 ps.

3.3. The dynamics of phase transition

In the initial condition, microcrystals having a rugged shape efficiently scatter the probe light. Correlation is measured with respect to this initial condition. From the fits to the data displayed in Fig. 5(b), we observe that there are at least three time constants to the changes in the correlation

function with time. Firstly, a fast decay (1.5 ns), then a fast rise (9 ns) and lastly a slow decay (15 ns). The initial loss of correlation arises from changes of morphology of DCNA microcrystals on the PEMA film probably due to rapid pump induced melting with a time constant of 1.5 ns (within the excitation pulse). The 9 ns component represents the recovery of correlation and indicates that the microcrystals reappear with this time constant in almost identical positions and with similar shapes. The longest component shown in Fig. 5(b) represents a permanent loss of correlation ending with a baseline that is not 1.00. This non-unit value of the base line indicates that some of the microcrystals or the polymer undergo permanent changes with a 15 ns time constant. The low amplitude of this component obviously leads to some error in the estimation of the time constant, but it can be clearly seen that the correlation is not fully recovered after 30 ns and, therefore, the end of the trace represents a permanent loss in correlation.

We explain events in the following manner. Under the present experimental conditions, DCNA molecules in the microcrystals are excited to their S_1 state during a single nanosecond pulse having a fluence of 250 mJ/cm^2. The electronically excited molecules release their acquired photon energy into intermolecular (phonon mode) and intramolecular vibrational modes via non-radiative processes. The local temperature surpasses the normal melting temperature and the microcrystals fuse. Smooth liquid surfaces scatter less light compared to the highly angular periodic structure of the microcrystals and the fast loss of correlation can, therefore, easily be explained by the phase transition from crystals to hot liquids. As shown in Figs. 3–5, although the vast majority of the microcrystals reappear, some crystals are permanently lost. The reappearance can be explained if the hot-melted DCNA liquid is rapidly cooled by dissipation of thermal energy into polymer with a 9 ns time constant resulting in recrystallization in the same position.

3.4. Dynamics of laser molecular dispersion and implantation

Laser molecular implantation and dispersion is represented by the long decay component with a time constant of 15 ns. This slow decay component leads to correlation loss that is not fully recovered giving a baseline of 0.97. We can estimate the amount of permanent crystal loss to be 20% by taking the ratio of amplitudes between the fitted transient and permanent changes in the correlation function in Fig. 5(b). Morphological change or crystal movement could result in a loss of correlation without crystal loss; therefore, in addition, we analyzed the ratio of the total scattering intensity between the polymer before and after excitation ($t = +\infty$) as depicted in the images in Fig. 4. This ratio was also 20% indicating that the changes in the correlation are due to permanent disappearance of crystals from the polymer surface. This being so we can consider that the permanent disappearance consists of two possible processes, these being vaporization of hot liquid into air and/or implantation from surface into polymer film. The recrystallization rate is faster than this slow component and this component should, therefore, involve some sublimation if vaporization is a prominent contribution to events. Since laser implantation of molecules into a polymer has been demonstrated under the same conditions, the slower component should be at least in part due to dispersion into the polymer. According to previous fluorescence studies of laser dispersion and implantation, 20% of molecules present as microcrystals on a polymer surface are implanted into polymer films by a single nanosecond laser pulse with a fluence of 250 mJ/cm^2 [15]. This coincidence between previous and present studies supports the assignment of dispersion and implantation as the slow depletion mechanism.

4. Conclusion

Using a ultramicroscope with 2 μm spacial resolution and 400 ps time resolution, we studied the laser-induced phase transition of the microcrystals on a polymer surface. After nanosecond pulsed laser excitation, 10 μm DCNA microcrystals become hot liquid droplets with a time constant of 1.5 ns. Subsequently, 80% of the droplets is recrystallized after cooling due to thermal energy dissipation with a time constant of 9 ns. Some amount of the microcrystals (20%) are permanently lost due to possible dispersion into the polymer film or evaporation with a time constant of 15 ns.

Acknowledgements

We thank Marubun Corporation (Tokyo, Japan) and La Vision GMBH (Göttingen, Germany) for generously providing the PicoStar ultrafast time-gated CCD camera. HF thanks Dr. Jonathan Hobley (Tohoku University) for valuable discussion and helpful comments on the manuscript. This work was partly supported by a Grant-in-Aid for Scientific Research (A)(2) from the Japanese Ministry of Education, Science, Sports and Culture (11355035).

References

[1] R. Srinivasan, B. Braren, Chem. Rev. 89 (1989) 1303.
[2] H. Kim, D.D. Dlott, J. Chem. Phys. 93 (1990) 1695.
[3] A. Tokmakoff, M.D. Fayer, D.D. Dlott, J. Phys. Chem. 97 (1993) 1901.
[4] D.D. Dlott, M.D. Fayer, J. Chem. Phys. 92 (1990) 3798.
[5] T. Lippert, A. Yabe, A. Wokaun, Adv. Mater. 9 (1997) 105.
[6] H. Fukumura, E. Takahashi, H. Masuhara, J. Phys. Chem. 99 (1995) 750.
[7] H. Fujiwara, H. Fukumura, H. Masuhara, J. Phys. Chem. 99 (1995) 11844.
[8] X. Wen, W. Tolbert, D.D. Dlott, J. Chem. Phys. 99 (1993) 4140.
[9] S. Chen, I.-Y.S. Lee, W.A. Tolbert, X. Wen, D.D. Dlott, J. Phys. Chem. 96 (1992) 7178.

[10] D.E. Hare, J. Franken, D.D. Dlott, J. Appl. Phys. 77 (1995) 5950.
[11] H. Fukumura, N. Mibuka, S. Eura, H. Masuhara, N. Nishi, J. Phys. Chem. 97 (1993) 13761.
[12] H. Fukumura, H. Kohji, N. Nagasawa, H. Masuhara, J. Am. Chem. Soc. 116 (1994) 10304.
[13] H. Fukumura, Y. Kohji, H. Masuhara, Appl. Surf. Sci. 96 (1996) 569.
[14] H. Fukumura, J. Photochem. Photobiol. A 106 (1997) 3.
[15] G. Gery, H. Fukumura, H. Masuhara, J. Phys. Chem. B 106 (1997) 3698.
[16] K. Saitow, N. Ichinose, S. Kawanishi, H. Fukumura, Chem. Phys. Lett. 291 (1998) 433.
[17] G. Gery, H. Fukumura, H. Masuhara, Chem. Commun. (1998) 811.
[18] B.J. Berne, R. Pecora, Dynamic Light Scattering, Wiley, New York, 1976.